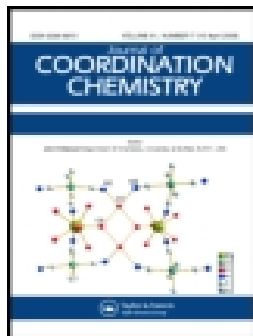


This is the peer-reviewed version of the following article:

Elshafly, H.; Bjelogrić, S. K.; Muller, C. D.; Todorović, T.; Rodić, M.; Marinković, A.; Filipović, N. R. Co(III) Complex with (E)-2-(2-(Pyridine-2-Ylmethylene)Hydrazinyl)-4-(4-Tolyl)-1,3-Thiazole: Structure and Activity against 2-D and 3-D Cancer Cell Models. *Journal of Coordination Chemistry* **2016**, 69 (22), 3354–3366.
<https://doi.org/10.1080/00958972.2016.1232404>.



This work is licensed under a [Creative Commons - Attribution-NonCommercial 2.0 Generic \(CC BY-NC 2.0\)](https://creativecommons.org/licenses/by-nc/2.0/)




Co(III) complex with (E)-2-(2-(pyridine-2-ylmethylene)hydrazinyl)-4-(4-tolyl)-1,3-thiazole: Structure and activity against two- and three-dimensional cancer cell model

Hana Elshafly, Snežana Bjelogrić, Christian D. Muller, Tamara R. Todorović, Marko Rodić, Aleksandar Marinković & Nenad R. Filipović

To cite this article: Hana Elshafly, Snežana Bjelogrić, Christian D. Muller, Tamara R. Todorović, Marko Rodić, Aleksandar Marinković & Nenad R. Filipović (2016): Co(III) complex with (E)-2-(2-(pyridine-2-ylmethylene)hydrazinyl)-4-(4-tolyl)-1,3-thiazole: Structure and activity against two- and three-dimensional cancer cell model, Journal of Coordination Chemistry, DOI: [10.1080/00958972.2016.1232404](https://doi.org/10.1080/00958972.2016.1232404)

To link to this article: <http://dx.doi.org/10.1080/00958972.2016.1232404>

 View supplementary material 

 Accepted author version posted online: 05 Sep 2016.
Published online: 05 Sep 2016.

 Submit your article to this journal 

 View related articles 

 View Crossmark data 

Publisher: Taylor & Francis

Journal: *Journal of Coordination Chemistry*

DOI: <http://dx.doi.org/10.1080/00958972.2016.1232404>

Co(III) complex with (*E*)-2-(2-(pyridine-2-ylmethylene)hydrazinyl)-4-(4-tolyl)-1,3-thiazole: Structure and activity against two- and three-dimensional cancer cell model

HANA ELSHAFLU^a, SNEŽANA BJELOGRLIĆ^b, CHRISTIAN D. MULLER^c, TAMARA R. TODOROVIĆ^d, MARKO RODIĆ^e, ALEKSANDAR MARINKOVIĆ^a and NENAD R. FILIPOVIĆ^{*f}

^aFaculty of Technology and Metallurgy, University of Belgrade, Karnegijeva 4, Belgrade, Serbia

^bNational Cancer Research Center of Serbia, Pasterova 14, Belgrade, Serbia

^cInstitut Pluridisciplinaire Hubert Curien, UMR 7178 CNRS, Faculté de Pharmacie, Université de Strasbourg, 67401 Illkirch, France

^dFaculty of Chemistry, University of Belgrade, Studentski trg 12-16, Belgrade, Serbia

^eDepartment of Chemistry, Faculty of Sciences, University of Novi Sad, Trg Dositeja Obradovića 4, Novi Sad, Serbia

^fFaculty of Agriculture, University of Belgrade, Nemanjina 6, Belgrade, Serbia

Co(III) complex with a 2-hydrazonylthiazole ligand was synthesized and characterized by single crystal X-ray diffraction. In the inner sphere of the complex two monoionic ligands are coordinated tridentate forming octahedral geometry around Co(III). Activity of the complex was investigated on MCF-7 breast cancer cell line, with cisplatin (CDDP) as a reference compound. Results showed that after 24 h incubation Co(III) complex revealed stronger cytotoxic activity compared to CDDP. Treatment of MCF-7 3-D cell model with the complex at 10 μ M concentration achieved complete suppression of spheroid growth in almost the same extent as at 100 μ M. In combination treatments on MCF-7 spheroids, the complex acted synergistically with CDDP, while additive interaction type was achieved when the complex was applied together with paclitaxel.

Keywords: Thiazoles; Co(III) complex; X-ray diffraction; Anticancer activity; Three drug combination study

*Corresponding author. Email: nenadf.chem@gmail.com

1. Introduction

Thiazole ring system is a pharmacophore found in major natural and synthetic biologically active compounds [1]. A vast number of 1,3-thiazole-based compounds were used as ligands due to their ability to coordinate various metal ions [2]. The coordination ability of 1,3-thiazole-based ligands is attributed to the presence of sulfur and nitrogen in the five-membered thiazole ring, but coordination capacity can be enhanced by structural modification and introduction of a variety of substituents with suitable donors [2]. (Thiazol-2-yl)hydrazones are a class of thiazoles which can be prepared by Hantzsch's reaction of thiosemicarbazones and α -haloarylcarbonyl compounds [2]. They showed antituberculosic, antifungal, antibacterial, antiparasitic, antioxidant and anticancer activities [3-7], and potent inhibitory activities against human monoamine oxidase B and histone acetyltransferase [8-10]. In this study, Co(III) complex with (thiazol-2-yl)hydrazone based HL (HL = 2-(2-pyridine-2-ylmethylene)hydrazinyl)-4-(4-tolyl)-1,3-thiazole) was synthesized. Apart from being a chemical element essential for normal metabolic function and a key substituent in Vitamin B12, cobalt was chosen as the central metal ion since its complexes often possess higher activities than cisplatin (CDDP) [11]. HL and its Co(III) complex were characterized by elemental analysis, nuclear magnetic resonance (NMR) and infrared (IR) spectroscopy, as well as single-crystal X-ray diffraction analysis. In this study we review results on anti-cancer activity of the Co(III) complex against human breast cancer MCF-7 cell line. Investigation has been performed on standard monolayer two-dimensional (2-D) cell culture model, and on three-dimensional (3-D) spheroid model which serves as a screening platform known to provide more reliable and meaningful therapeutic readouts compared to 2-D tests [12]. Also, activities and type of drug interactions on 3-D model subjected to combination treatment with Co(III) complex and CDDP or paclitaxel, as well as all three drugs in combination were evaluated. This is the first three-drug combination study carried out on a 3-D cell culture to date.

2. Experimental

2.1. General remarks

Thiosemicarbazide (99%), 2-pyridinecarboxaldehyde (99%) and 2-bromo-4'-methylacetophenone were obtained from Acros Organics (BVBA, Geel, Belgium). Cobalt tetrafluoroborate hexahydrate was obtained from Aldrich (Sigma-Aldrich Chemie GmbH,

Steinheim, Germany). All solvents (reagent grade) were obtained from commercial suppliers and used without purification. Elemental analyses (C, H and N) were performed by the standard micromethods using the ELEMENTARVario ELIII C.H.N.S=O analyzer. Infrared (IR) spectra were recorded on a Thermo Scientific Nicolet 6700 FT-IR spectrophotometer by the attenuated total reflection (ATR) technique from 4000–400 cm^{-1} . Molar conductivity measurement was performed at ambient temperature on a Crison Multimeter MM41. The 1-D (^1H and ^{13}C) and 2-D NMR spectra were performed on Bruker Avance 500, equipped with a broad-band direct probe. All spectra were measured at 298 K. Chemical shifts are given on δ scale relative to tetramethylsilane (TMS) as internal standard for ^1H and ^{13}C . Atom numbering used in NMR is shown in scheme 1.

2.2. Synthesis of (*E*)-2-(2-(pyridine-2-ylmethylene)hydrazinyl)-4-(4-tolyl)-1,3-thiazole (HL)

2-Formylpyridine thiosemicarbazone (Hfptsc) was synthesized according to the reported literature procedure [6]. 2-Bromo-4'-methylacetofenone (0.1928 g, 8.1 mmol) was added into suspension of Hfptsc (0.1460 g, 8.1 mmol) in 20 mL H_2O / EtOH mixture (1 : 1, v/v) and stirred for 3 h at room temperature. Yellow precipitate was filtered off and washed three times with H_2O and EtOH. Single crystals of HL suitable for single crystal X-ray diffraction were obtained by slow diffusion of MeCN vapour into DMSO solution of raw product. Crystals were filtered off and washed with cold MeCN. Yield: 0.150 g (63%). Anal. Calcd for $\text{C}_{16}\text{H}_{14}\text{N}_4\text{S}$ (%): C, 65.28; H, 4.79; N, 19.09; S, 10.89. Found: C, 65.46; H, 4.84; N, 18.99; S, 10.46. IR (ATR, $\nu_{\text{max}}/\text{cm}^{-1}$): 3176 (w), 3109 (w), 3066 (w), 2930 (w), 2850 (w), 2717 (m), 1599 (m), 1573 (vs), 1478 (s), 1456 (w), 1431 (w), 1407 (w), 1360 (w), 1298 (w), 1271 (vs), 1148 (s), 1115 (w), 1089 (w), 1047 (m), 1000 (m), 913(m), 879 (w), 839 (w), 789 (w), 766 (w), 726 (m), 681 (m), 637 (w). ^1H NMR (500.26 MHz, DMSO-d_6), δ_{H} : 2.31, (s, 3H, H-C16), 7.21 (d, 2H, H-C6 = H-C8, $^3J_{6,5} = ^3J_{8,9} = 8.0$ Hz), 7.27 (s, 1H, H-C2), 7.34 (m, 1H, H-C14), 7.75 (d, 2H, H-C5 = H-C9, $^3J_{5,6} = ^3J_{9,8} = 8.0$ Hz), 7.84 (m, 1H, H-C12), 7.85 (m, 1H, H-C13), 8.07 (s, 1H, H-C10), 8.57 (m, 1H, H-C15), 12.40 (br.s, N-H). ^{13}C NMR (126.0 MHz, DMSO-d_6) δ_{C} : 20.78 (C16), 103.22 (C2), 119.13 (C12), 123.57 (C14), 125.46 (C5 = C9), 129.18 (C6 = C8), 131.91 (C4), 136.88 (C7), 136.88 (C13), 141.41 (C10), 149.43 (C15), 150.71 (C3), 153.24 (C11), 167.70 (C1).

2.3. Synthesis of $[Co(L)_2]BF_4$ (**1**)

Into suspension of HL (0.10 g; 0.34 mmol) in 20 mL of MeOH, solid $Co(BF_4)_2 \cdot 6H_2O$ (0.58 g, 0.17 mmol) was added and the rotten cherry solution was refluxed for 1 h. After two days emerald colored single crystals of **1** were filtered off, washed with cold MeOH and Et_2O . Yield: 0.07 g (57%). Anal. Calcd for $C_{32}H_{26}N_8S_2CoBF_4$ (%): C, 52.47; H, 3.58; N, 15.30; S, 8.76. Found: C, 52.46; H, 3.39; N, 15.40; S, 8.84. Λ_M (1×10^{-3} M, MeOH) = $89.10 \Omega^{-1} cm^2 mol^{-1}$. IR (ATR, ν_{max}/cm^{-1}): 3548 (w), 3128 (w), 3074 (w), 1603 (m), 1570 (w), 1533 (s), 1486 (m), 1444 (w), 1400 (vs), 1346 (vs), 1326 (w), 1245 (s), 1136 (w), 1055 (m), 935 (w), 906 (m), 846 (w), 811 (m), 766 (m), 676 (w), 637 (w). 1H NMR (500.26 MHz, DMSO- d_6) δ_H : 2.46 (s, 3H, H-C16), 6.50 (s, 1H, H-C2), 6.64 (d, 2H, H-C6 = H-C8, $^3J_{6,5} = ^3J_{8,9} = 8.0$ Hz), 7.21 (d, 2H, H-C5 = H-C9, $^3J_{5,6} = ^3J_{9,8} = 8.0$ Hz), 7.28 (ddd, 1H, H-C13, $^3J_{13,12} = 5.7$ Hz, $^3J_{13,14} = 7.4$ Hz), 7.65 (dd, 1H, H-C14, $^3J_{14,15} = 7.9$ Hz), 7.82 (s, 1H, H-C10), 7.84 (d, 1H, H-C12, $^3J_{12,13} = 5.7$ Hz), 7.99 (td, 1H, H-C15, $^3J_{15,14} = 7.9$ Hz). ^{13}C NMR (126.0 MHz, DMSO- d_6) δ_C : 21.19 (C16), 107.98 (C2), 123.22 (C12), 125.98 (C14), 128.22 (C5 = C9), 128.66 (C6 = C8), 128.84 (C4), 138.90 (C7), 139.35 (C13), 141.01 (C10), 148.01 (C15), 149.12 (C3), 159.91 (C11), 180.43 (C1).

2.4. X-ray crystallography

Single crystal X-ray diffraction was performed on an Oxford Diffraction Gemini S kappa geometry diffractometer, equipped with Mo $K\alpha$ radiation ($\lambda = 0.710689 \text{ \AA}$) from a sealed tube source, and a Sapphire CCD detector. Data collection strategy calculation, data reduction, cell refinement and absorption correction were performed with CRYCALISPRO [13]. The structure was solved using SHELXT [14] and refined with anisotropic displacement parameters for all non-hydrogen atoms using SHELXL-2014/6 [15]. Program SHELXLE [16] was used as graphical user interface for structure solution and refinement procedures. Hydrogens bonded to carbons in HL and **1** were introduced in idealized positions and refined using a riding model. Hydrogens bonded to nitrogen were located by difference Fourier synthesis and refined using distance restraints with U_{iso} approximated by $1.2U_{eq}$ of the parent atoms in HL. Complex **1** was found to crystallize in non-centrosymmetric space group. The absolute configuration is determined by the Flack-parameter [17]. Structures were validated using PLATON [18] and Cambridge Structural Database (v. 5.37, updates Feb. 2016) [19] using MERCURY CSD [20].

2.5. Biological experiments

2.5.1. Cell cultures. Human mammary adenocarcinoma (MCF-7, ATCC® HTB-22) cell line was maintained in DMEM high glucose medium (Dominique Dutscher, 67172 Brumath cedex, France, Cat. No. L0102-500), supplemented with heat-inactivated 10% (v/v) fetal bovine serum (FBS, Life Technologies, Paisley, UK, Cat. No. 10270-106) and 1% (v/v) penicillin-streptomycin (10,000 units mL⁻¹ and 10,000 µg mL⁻¹, Life Technologies, Paisley, UK, Cat. No. 15140-122). Cells were kept at 37 °C in humidified atmosphere containing 5% (v/v) CO₂ during their exponential growing phase and in the course of incubation with investigated compounds. **1** was initially dissolved in DMSO to the stock concentration of 20 mM, whereas CDDP and starting cobalt salt were dissolved in phosphate buffer saline (PBS) to the stock concentration of 5 mM. Further dilutions of the compounds were performed with DMEM medium immediately before each experiment. HL could not be tested due to low solubility in the culture medium.

2.5.2. Annexin-V / propidium iodide (PI) double staining and determination of ED₅₀ concentrations on 2-D tumor model. MCF-7 cells were seeded in flat bottom 96 well plates (BD Falcon, Cat. No. 353072) at a density of 10,000 cells per 0.1 mL of media. Next day, CDDP, **1** and starting cobalt salt were added in a range of six concentrations (1–100 µM), in a volume of 0.1 mL. For controls, non-treated cells, cells treated with 0.5% DMSO and cells treated with 50 µM Celastrol (Enzo Life Sciences, Farmingdale, US) were used. After 24 h of incubation, supernatant with non-adherent cells were removed to another plate. Fresh PBS was added to remaining adherent cells; afterwards plates were centrifuged on 450 g for 10 min. Supernatant was discarded and 200 µL of trypsin-EDTA (BioWest, Nuaille, France, Cat. No. L0930-100) was added to each well. Cells were detached in about 15 min of incubation at 37 °C; afterwards another spinning cycle with supernatant elimination was performed. Finally, previously removed supernatant with non-adherent cells were added to trypsinized cells and stained with Annexin-V-FITC (Immuno Tools, Friesoythe, Germany, Cat. No. 31490013) and PI (Miltenyl Biotec Inc., Auburn, USA, Cat. No. 130-093-233) in volumes of 3 µL. Plates were analyzed on a Guava EasyCyte™ micro-capillary flow cytometer (Millipore, Merck, Darmstadt, Germany) using InCyte® software package. Percentages of all cell death events (Annexin-V single-stained, PI single-stained and double-stained cells) were summarized for each of the six

concentrations. The computed percentages were plotted against corresponding concentrations on a concentration-response graph. ED₅₀ concentration was calculated as the one that corresponds to half-way of the sigmoidal concentration-dependent curve using asymmetric five-parameter logistic equation (GraphPad Prism 6 software).

2.5.3. Evaluation of a single-drug activity on 3-D tumor model. 3-D MCF-7 mamospheres were made in 96 well plates (Corning, Sigma-Aldrich, St. Louis, MO, USA, Cat. No. 4515). Tumors were left to grow for an additional four days; afterwards CDDP and **1** were added in concentrations of 100, 10 and 1 μ M. Evaluation has been maintained during an eight day incubation period, with media exchanged on day four. Changes in the tumor sizes have been assessed on a Celigo[®] imaging cytometer (Cytellect, Brooks Life Science Systems, Poway, CA, USA) using Celigo software. Spheroid areas were determined using Celigo software, and growth rates were computed for every other day of incubation by dividing the area on the day-n with the area on the day 0.

2.5.4. Evaluation of a combination drug activity on 3-D tumor model. Spheroids were prepared as described above, and after four days growth drugs were added in combinations. Complex **1** was tested in combination with CDDP and paclitaxel, respectively, and together as a three drug combination, with the single-drug treated spheres as positive controls for each drug in a combination. Treatments lasted for eight days with exchange of media on the fourth day. Changes in sizes of spheres were assessed as described above for days zero, four, and eight of incubation. Computed growth rates for day eight were used to determine the type of interaction between drugs in combinations expressed as combination indexes (CI) using CalcuSyn software (Biosoft, Cambridge, United Kingdom). The CI value defines the type of interaction between drugs as following: for CI < 0.9 interaction is synergistic, for 0.9 < CI < 1.1 interaction is additive, and for CI > 1.1 interaction is antagonistic.

3. Results and discussion

3.1. Synthesis and spectroscopic characterization

Preparation of HL hydrogen bonded Z-isomer was previously published [6]. In this work E-isomer of the HL ligand was prepared by Hantzsch's reaction of Hfptsc and 2-bromo-4'-

methoxyacetophenone in a H₂O/EtOH mixture (scheme 1). By reaction of HL and Co(BF₄)₂·6H₂O in MeOH, [Co(L)₂]BF₄ (**1**) was obtained (scheme 1). HL and **1** are soluble in DMF and DMSO at room temperature, and in EtOH, MeOH and MeCN at elevated temperature. Results of the elemental analysis suggested that in **1** there are two deprotonated ligand molecules, cobalt ion and one tetrafluoroborate. The composition of **1** is in accord with the result of conductivity measurement.

The IR spectrum of HL (figure S1, Supplementary data) contains several characteristic bands. The band at 3176 cm⁻¹ can be attributed to ν(N-H). The ligand exhibits a broad band around 2700 cm⁻¹ which is assigned to the intermolecular H-bonding vibrations noticed in the solid state (*vide infra*). Bands at 1599 and 1573 cm⁻¹ are assigned to ν(C=N) of azomethine group and thiazole ring, respectively. Coordination of azomethine nitrogen can be assumed on the basis of the shift of the band originating from ν(C=N) of azomethine toward higher frequency in the complex (1603 cm⁻¹), while the band originating from ν(C=N) of thiazole ring is shifted to lower frequency in the IR spectrum of the complex (1533 cm⁻¹). The intensities of these bands decreased. Also, in the IR spectrum of the complex (figure S2, Supplementary data) a strong band at 1055 cm⁻¹, originating from non-coordinated tetrafluoroborate, can be seen.

HL and **1** were characterized by ¹H and ¹³C NMR spectroscopy (figures S3–S6, Supplementary data) with spectral data given in the Experimental Section. In ¹H NMR spectrum of **1** the signal from H–N proton (at 12.40 ppm in the ligand) is missing, indicating coordination of the ligand in its deprotonated form. Coordination *via* nitrogen from thiazole ring could be evidenced by strong upfield ¹H NMR shift of H–C2 and also by downfield of ¹³C NMR shift of C1 and C2 signals with respect to the ligand. Azomethine nitrogen coordination is supported by the upfield shift of H–C10 proton and downfield shift of C11 signals, while pyridine nitrogen coordination can be evidenced by upfield shifts of H–C13 and H–C15 protons and downfield shift of C13 signal with respect to the ligand.

3.2. Crystal structure analysis

Crystal data and refinement results for HL and **1** are summarized in table 1, while molecular structures are depicted in figure 1. The ligand is planar within 0.18 Å and adopts a conformation in which pyridine N4 and azomethine N3, and azomethine N3 and thiazole N1 are mutually in *trans* positions [figure 1(a)]. This implies conformational rearrangement is necessary for

tridentate metal binding. Crystal structure of HL [figure 1(b)] is dominated by hydrogen bonds between the N4H groups and pyridine nitrogen that give 1-D chains along the *b*-axis. The stacking interactions between neighboring pyridine and tolyl fragments expand these 1-D chains into 2-D supramolecular layers parallel to (001) [figure 1(c), table 2].

Spontaneous resolution of the racemate occurs during crystallization of **1**, so that the compound crystallizes as a mixture of enantiopure crystals (conglomerate) in non-centrosymmetric space group $P2_12_12_1$. Thus, each individual crystal contains only one optical isomer of $[\text{CoL}_2]^+$. Octahedral complex cation in **1** is comprised of two meridionally placed ligand molecules chelating Co(III) and possesses approximate two-fold symmetry [figure 2(a)]. HL molecules are coordinated in an anionic form as tridentate NNN donors, through the pyridine, azomethine and thiazole nitrogens. Distortion from an ideal octahedral geometry in **1** is imposed by the ligands' bite angles. In the crystal structure of **1** [figure 2(b)], in addition to the electrostatic attraction, cations and tetrafluoroborate anions are connected through hydrogen bonds (table 2).

3.3. Comparison of anticancer activity on 2-D and 3-D cell models

Investigation on anti-cancer activity of **1** was initiated by evaluation of its ability to induce cell death in a classical MCF-7 2-D monolayer culture over 24 h of incubation. CDDP was chosen as our reference compound, as it is currently the most efficient metal complex administered in treatments of various types of cancer [21]. The activity of HL could not be tested due to its low solubility in the cell culture medium. Starting cobalt salt after 24 h of incubation exhibited very low cytotoxic activity and did not reach ED₅₀ value in the range of applied concentrations (up to 100 μM). As represented in figure 3, treatment with **1** induced higher incidence of cell death compared to CDDP. Contrary to CDDP, activity of **1** displayed a wide plotted concentration-response curve. This implies there is a broad concentration of **1** to achieve the desired treatment effect while avoiding a toxic threshold, *i.e.* a characteristic of a drug of good therapeutic index [22].

The next step was to examine the activity of **1** and CDDP in a 3-D cell model. 3-D culture models are *in vitro* derived tissues which mimic *in vivo* tumors with respect to gradient of nutrients, oxygen and metabolites within themselves [23]. Therefore, 3-D models serve as a screening platform for drug effectiveness in a function of multiple parameters such as drug

concentration, molecular weight, kinetics, charge, solubility, diffusion, metabolism, and sequestration [24]. Changes in 3-D cultures can be analyzed regarding two parameters: size and morphology. Due to insufficiency of mass transport through cellular barriers, there are three concentric zones clearly distinguished within newly developed spheroid: necrotic core (black circle located in the center of sphere, consisting of dead cells), quiescent zone (transparent dark gray rim that surrounds necrotic core), and proliferating zone (transparent light gray located on the outer edge). Sizes and mutual ratio of these zones altered over the days of incubation, thus in non-treated spheroids necrotic core is getting bigger with quiescent zone significantly thinned and completely suppressed to the very edge of the sphere (figure 4).

Spheroids treated with CDDP showed concentration-dependent changes in both parameters (figure 4). Concentration of 100 μM induced reduction in spheroid size after second day of incubation, together with markedly expanded necrotic core and loss of proliferating zone. Size of those spheroids remained unchanged over the time of incubation, but zones became unrecognizable with development of strikingly crispy edges. CDDP at concentration of 10 μM induced growth regression almost equivalent to that achieved with 100 μM , but morphological transformation was far less prominent. Thus, on the fourth day, 3-D cultures subjected to concentration of 10 μM still had a well-defined edge and preserved thin proliferation zone. Spheroids incubated with 1 μM of CDDP were the least affected in both growth rate and morphological changes.

The highest (100 μM) applied concentration of **1** initially induced an increase in size of 3-D culture accompanied with complete loss of recognizable zones within its architecture, demonstrating mighty drug activity. Starting on the fourth incubation day, those spheroids were displaying a decrease in size, thus on day eight, their growth rate was almost equal to the one obtained after CDDP treatment at the same concentration (1.08 ± 0.03 and 0.95 ± 0.01 for **1** and CDDP, respectively). Spheroids incubated with a median concentration of **1** (10 μM) were gradually losing their zonal segregation. At day two, a necrotic core was still distinctive, while the quiescent zone was dark and glazy with complete disappearance of any proliferation rim. Two days later, the necrotic core could be barely identified, while on day six, spheroid zonal organization was completely obliterated. Nevertheless, those two concentrations of **1** induced almost the same activity on 3-D cultures, but morphological transformations registered in spheroids treated with concentration of 10 μM were vigorous to a lesser extent. As for CDDP,

the lowest tested concentration of **1** (1 μM) did not produce any substantial growth rate inhibition. However, due to the delayed growth, the ratio between necrotic core and quiescent zone at day eight was approximately the same as seen on day four in control 3-D cultures.

The differences in response to treatment with **1** on monolayer or spheroids at 10 and 100 μM provide insight into benefit of drug testing on a 3-D model. Since 2-D culture of adherent cells is considered as completely unrealistic formation where all cells are equally exposed to applied treatment, it is not surprising that promising results gained from *in vitro* evaluation are frequently not confirmed during *in vivo* assessment. Here, concentration of 10 μM achieved almost the same activity on the 3-D model as concentration of 100 μM on 2D, a result completely unforeseen according to percentages of cell death scored with those concentrations on 2-D [figures 3 and 4(a)]. Thus, our results confirm that **1** is a compound with potentially high therapeutic index, and by careful dose titration, the desired impact should not be compromised with side effects.

3.4. Combination treatment

The strategy of combination treatment implies acting upon different targets in order to improve therapeutic effect as well as to interfere with development of drug resistance which tumor cells can easily acquire in case of single drug therapy. Major disadvantage of combination treatment includes interactions at the level of side effects. Such interaction demands dose reduction for each drug given in combination so to avoid serious toxic complications. We evaluated here the possibility of interaction of **1** with paclitaxel, one of the most used drugs for treatment of breast cancer [25]. On the other hand, CDDP was revealed as effective for the treatment of locally advanced breast cancer, metastatic breast cancer and triple-negative breast cancers [26].

The least effective concentrations of **1** and CDDP confirmed in the single-treatment experiment were used (1 μM , figure 4) in planning of combination treatments in respect of the general approach that implies dose reduction of drugs in combination, while paclitaxel was investigated in concentration of 1 nM also determined as the concentration with lowest activity in the tested range between 1-100 nM (data not shown). As shown in figure 5, combination of paclitaxel with **1** was the least effective when compared to other three combinations. However, the true type of interaction within combinations becomes evident when represented by the combination index [CI, figure 5(c)]. Combination of **1** with CDDP revealed synergistic

interaction whereas **1** in combination with paclitaxel acted additively with less efficient inhibition of spheroid growth. CDDP with paclitaxel in combination performed synergistically against MCF-7 3-D model, while the addition of **1** to the triple combination did not help to gain any improvement of the overall effect of two conventional drugs, but additionally did not reduce it either. Different type of interactions defined for **1** and CDDP when they were separately combined with paclitaxel remains a strong indication that those two metal complexes do not share the same target. Their combination deserves further investigation on this and other 3-D models tested in various concentration ratios.

4. Conclusion

Although HL is a thiazole - a class of organic compounds with high biological activity, its activity could not be tested here due to the low solubility in culture medium (of high sodium salt content). Reactions with metal ions can influence the solubility of the ligand itself. We have here synthesized and characterized a *d*-metal complex with (thiazol-2-yl)hydrazone ligand. The obtained Co(III) complex **1** is a 1:1 electrolyte, soluble in DMSO and used culture medium, thus suitable for biological experiments. Anticancer activity of **1** was investigated using the standard monolayer 2-D and 3-D spheroid model, where the latter provides more accurate assessment of investigated compound's actual impact on tumor growth inhibition. Our results reveal that **1** is a more potent inducer of cell death than CDDP after 24 h incubation on MCF-7 2-D model, whereas both drugs achieved inhibition of 3-D MCF-7 spheres growth in almost the same extent after eight days of incubation. However, the difference in morphological changes of spheroids subjected to CDDP and **1** was the primary indication that those two compounds do not share the same mechanism of activity, supported by the results of combination treatment. The evidence that these two metal complexes in combination resulted in synergistic interaction might, at first glance, discard the assumption stated above. However, their discordant interaction with paclitaxel contributed to hypothesize on the diversity of CDDP and **1** mechanisms for their anticancer effect. Although this is the first study on anticancer property of **1**, current results strongly approve its further testing onto other cancer models, especially the underlying mechanism of synergistic interaction with CDDP.

Appendix A. Supplementary data

CCDC 1441009 and CCDC 1441010 contain the supplementary crystallographic data for HL and 1, respectively. This data can be obtained free of charge via <https://summary.ccdc.cam.ac.uk/structure-summary-form>, or from the Cambridge Crystallographic Data Centre, 12 Union Road, Cambridge CB2 IEZ, UK; Fax: (+044)1223-336-033; or E-mail: deposit@ccdc.cam.ac.uk. Supplementary data associated with this article can be found in the online version.

Acknowledgements

The Ministry of Education, Science and Technological Development of the Republic of Serbia under Grants 172055 and 172013 supported this work. The authors acknowledge networking support by the COST Action CM1106 StemChem – “Chemical Approaches to Targeting Drug Resistance in Cancer Stem Cells”.

References

- [1] A. Rauf, N.N. Farshori, In *Microwave-Induced Synthesis of Aromatic Heterocycles*, S.K. Sharma (Ed.), Chap. 3, pp. 15–19, Springer, Netherlands (2012).
- [2] L.M.T. Frija, A.J.L. Pombeiro, M.N. Kopylovich. *Coord. Chem. Rev.*, **308**, 32 (2016).
- [3] A. Arshad, H. Osman, M.C. Bagley, C.K. Lam, S. Mohamad, A.S.M. Zahariluddin. *Eur. J. Med. Chem.*, **46**, 3788 (2011).
- [4] A.M. Vijesh, A.M. Isloor, V. Prabhu, S. Ahmad, S. Malladi. *Eur. J. Med. Chem.*, **45**, 5460 (2010).
- [5] F. Chimenti, B. Bizzarri, A. Bolasco, D. Secci, P. Chimenti, S. Carradori, A. Granese, D. Rivanera, N. Frishberg, C. Bordon, L. Jones-Brando. *J. Med. Chem.*, **52**, 4574 (2009).
- [6] M.V. de Oliveira Cardoso, L.R. Pessoa de Siqueira, E.B. da Silva, L.B. Costa, M.Z. Hernandez, M.M. Rabello, R.S. Ferreira, L.F. da Cruz, D.R.M. Moreira, V.R.A. Pereira, M.C.A.B. de Castro, P.V. Bernhardt, A.C.L. Leite. *Eur. J. Med. Chem.*, **86**, 48 (2014).
- [7] M.H Shih, Y.S. Su, C.L. Wu. *Chem. Pharm. Bull.*, **55**, 1126 (2007).
- [8] P. Chimenti, A. Petzer, S. Carradori, M. D’Ascenzio, R. Silvestri, S. Alcaro, F. Ortuso, J.P. Petzer, D. Secci. *Eur. J. Med. Chem.*, **66**, 221 (2013).

- [9] F. Chimenti, E. Maccioni, D. Secci, A. Bolasco, P. Chimenti, A. Granese, O. Befani, P. Turini, S. Alcaro, F. Ortuso, M.C. Cardia, S. Distinto. *J. Med. Chem.*, **50**, 707 (2007).
- [10] F. Chimenti, B. Bizzarri, E. Maccioni, D. Secci, A. Bolasco, P. Chimenti, R. Fioravanti, A. Granese, S. Carradori, F. Tosi, P. Ballario, S. Vernarecci, P. Filetici. *J. Med. Chem.*, **52**, 530 (2009).
- [11] C.R. Munteanu, K. Suntharalingam. *Dalton Trans.*, **44**, 13796 (2015).
- [12] Y.C. Tung, A.Y. Hsiao, S.G. Allen, Y.S. Torisawa, M. Ho, S. Takayama. *Analyst*, **136**, 473 (2011).
- [13] CrysAlisPro Software system, Agilent Technologies UK Ltd., Oxford (2014).
- [14] G.M. Sheldrick. *Acta Crystallogr.*, **A71**, 3 (2015).
- [15] G.M. Sheldrick. *Acta Crystallogr.*, **C71**, 3 (2015).
- [16] C.B. Hübschle, G.M. Sheldrick, B. Dittrich. *J. Appl. Crystallogr.*, **44**, 1281 (2011).
- [17] S. Parsons, H. Flack, T. Wagner. *Acta Crystallogr.*, **B69**, 249 (2013).
- [18] A.L. Spek. *Acta Crystallogr.*, **D65**, 148 (2009).
- [19] F.H. Allen. *Acta Crystallogr.*, **B58**, 380 (2002).
- [20] C.F. Macrae, I.J. Bruno, J.A. Chisholm, P.R. Edgington, P. McCabe, E. Pidcock, L. Rodriguez-Monge, R. Taylor, J. van de Streek, P.A. Wood. *J. Appl. Crystallogr.*, **41**, 466 (2008).
- [21] L. Kelland. *Nat. Rev. Cancer*, **7**, 573 (2007).
- [22] P.Y. Muller, M.N. Milton. *Nat. Rev. Drug Discov.*, **11**, 751 (2012).
- [23] D.R. Grimes, C. Kelly, K. Bloch, M. Partridge. *J. R. Soc. Interface*, **11**, 1124 (2013).
- [24] R.-Z. Lin, H.-Y. Chang. *Biotechnol. J.*, **3**, 1172 (2008).
- [25] S. Griffin, G. Dunn, S. Palmer, K. Macfarlane, S. Brent, A. Dyker, S. Erhorn, C. Humphries, S. White, W. Horsley, L. Ferrie, S. Thomas. *Health Technol. Assess.*, **13**, 15 (2009).
- [26] B.S. Yadav, S.C. Sharma, P. Chanana, S. Jhamb. *World J. Clin. Oncol.*, **5**, 125 (2014).

Table 1. Data collection and refinement parameters for crystal structures of HL and **1**.

	HL	1
Chemical formula	C ₁₆ H ₁₄ N ₄ S	C ₃₂ H ₂₆ BCoF ₄ N ₈ S ₂
Formula weight	294.37	732.47
Temperature (K)	294	294
Wavelength (nm)	0.71073	0.71073
Crystal system	Monoclinic	Orthorhombic
Space group	<i>P2₁/c</i>	<i>P2₁2₁2₁</i>
<i>a</i> , <i>b</i> , <i>c</i> (Å)	7.9329(4), 8.6465(3), 21.5857(9)	9.8152(3), 15.3902(5), 22.2103(5)
α , β , γ (°)	90, 99.822(4), 90	90, 90, 90
<i>V</i> (Å ³)	1458.90(11)	3355.04(17)
<i>Z</i>	4	4
μ (mm ⁻¹)	0.22	0.70
Crystal size (mm)	0.70 × 0.17 × 0.07	0.20 × 0.14 × 0.09
<i>T</i> _{min} , <i>T</i> _{max}	0.922, 0.986	0.895, 0.946
No. of measured, independent and observed [<i>I</i> > 2σ(<i>I</i>) reflections	12639 3489 2755	13706 7148 4887
<i>R</i> _{int}	0.026	0.061
(sin θ/λ) _{max} (Å ⁻¹)	0.680	0.683
<i>R</i> [<i>F</i> ² > 2σ(<i>F</i> ²)]	0.041	0.074
<i>wR</i> (<i>F</i> ²)	0.132	0.188
<i>S</i>	1.08	1.06
No. of reflections	3489	7148
No. of parameters	195	436
Δ _{max} , Δ _{min} (e Å ⁻³)	0.31, -0.37	0.63, -0.69
Absolute structure	/	Flack <i>x</i> determined using 1621 quotients [(<i>I</i> +) - (<i>I</i> -)] / [(<i>I</i> +) + (<i>I</i> -)] ^[ref. 16]
Absolute structure parameter	/	-0.018 (12)

Table 2. Crystal packing parameters in the crystal structures of HL and **1**.

HL: H-bond parameters					
D–H...A	D–H (Å)	H...A (Å)	D...A (Å)	D–H...A (°)	symmetry operation on A
N2–H2...N4	0.87(3)	2.05(3)	2.915(2)	175(2)	$1-x, 1/2+y, 1/2-z$
HL: π - π interaction parameters					
Cg(I),Cg(J) ^a	α^c (°)	β^d (°)	γ^e (°)	slippage ^f (Å)	symmetry operation on J
Cg–Cg ^b (Å)					
Cg1, Cg2	6	16.9	22.6	1.094	$-1+x, -1+y, z$
3.7633(10)					
1 : H-bond parameters					
D–H...A	D–H (Å)	H...A (Å)	D...A (Å)	D–H...A (°)	symmetry operation on A
C2–H2...F3	0.93	2.44	3.316(14)	158	$2-x, 1/2+y, 3/2-z$
C10–H10...F4	0.93	2.34	3.236(11)	162	$3/2-x, 1-y, -1/2+z$
C10A–H10A...F1	0.93	2.50	3.405(10)	163	$-1+x, y, z$
C12–H12...F1	0.93	2.48	3.395(11)	171	$3/2-x, 1-y, -1/2+z$

^a Planes of the rings I/J: ring (1) = N(4),C(11),C(12),C(13),C(14),C(15); ring (2) = C(4),C(5),C(6),C(7),C(8),C(9)

^b Cg–Cg = distance between ring centroids (Å).

^c α = dihedral angle between planes I and J (°).

^d β = angle between Cg(I),Cg(J) vector and normal to plane I (°).

^e γ = angle between Cg(I), Cg(J) vector and normal to plane J (°).

^f Slippage = distance between Cg(I) and perpendicular projection of Cg(J) on ring I (Å).

Figure captions

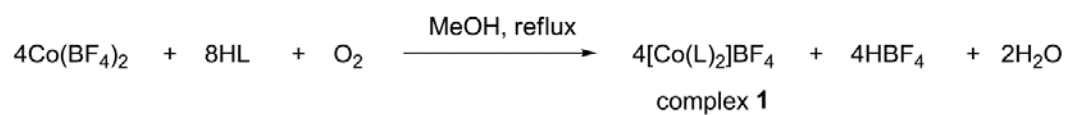
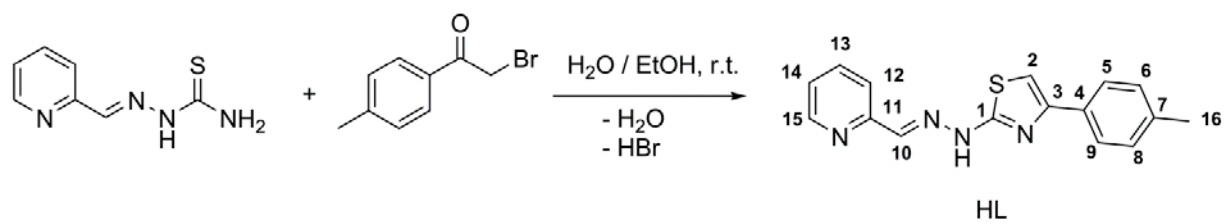
Figure 1. (a) Perspective view and labeling of the molecular structure of HL. Thermal ellipsoids are at the 40% probability level. Selected bond lengths (Å) and angles (°) with SD's in parentheses: N4–C11, 1.342(2); C10–C11, 1.465(2); N3–C10, 1.277(2); N2–N3, 1.3604(19); C1–N2, 1.362(2); N1–C1, 1.300(2); S1–C1, 1.7382(17); S1–C2, 1.7231(19); C2–C3, 1.357(2); C2–S1–C1, 87.88(8); C1–N1–C3, 109.99(13); N1–C1–N2, 123.79(15); N1–C1–S1, 116.05(12); N2–C1–S1, 120.15(12); N3–N2–C1, 116.98(14); C3–C2–S1, 111.26(13); C10–N3–N2, 117.63(14); N3–C10–C11, 119.78(15). (b) Infinite 1-D chains in the crystal structure of HL viewed along the *a*-axis. (c) 2-D supramolecular layers in the crystal structure of HL viewed along the *c*-axis.

Figure 2. (a) Perspective view and labeling of the molecular structure of [CoL₂]⁺ in **1**. Thermal ellipsoids are at the 40% probability level. Selected bond lengths (Å) and angles (°) with SD's in parentheses: Co1–N1, 1.938(6); Co1–N1A, 1.949(6); Co1–N3, 1.888(5); Co1–N3A, 1.885(5); Co1–N4, 1.954(6); Co1–N4A, 1.937(6); N2–N3, 1.352(9); N2A–N3A, 1.335(8); N3–C10, 1.290(10); N3A–C10A, 1.280(10); N2–C1, 1.326(10); N2A–C1A, 1.326(9); S1–C1, 1.726(9); S1–C2, 1.731(9); S1A–C1A, 1.728(7); S1A–C2A, 1.718(10); N1–C1, 1.356(9); N1–C3, 1.370(9); N1A–C1A, 1.336(9); N1A–C3A, 1.395(10). (b) Crystal packing in the crystal structure of **1** viewed along the *a*-axis. Hydrogens are omitted for clarity.

Figure 3. Concentration-response curves and ED₅₀ values for **1** (a) and CDDP (b) on 2-D MCF-7 cell model after 24 h of incubation. Results are presented as percentage of cell death events determined by Annexin-V/PI double staining in two independent experiments (open and closed circles) and asymmetric five-parameter sigmoidal curve computed for both replicates in GraphPad Prism software.

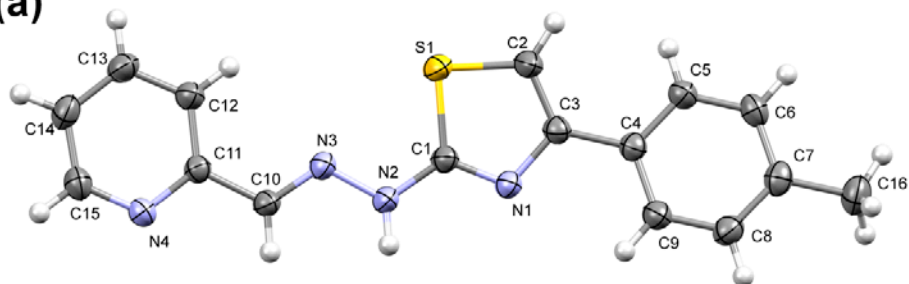
Figure 4. (a) MCF-7 3-D culture changes in growth and morphology induced by the treatment with either **1** or CDDP added in three concentrations over the 8-day incubation period. Images have been acquired every other day, starting from day 0 on the Celigo imaging cytometer using Celigo software. Scale bar: 500 μm. (b) Changes in growth rate of MCF-7 spheroids treated with either **1** or CDDP applied in concentrations of 100 μM (open circle), 10 μM (full square), and 1 μM (open square), and non-treated control (full circle). Growth rate was determined by means of spheroid area established with Celigo software, and afterwards computed for every other day of the 8-day incubation period by dividing the area on the day-*n* with the area on the day 0. Results are presented as the mean ± SD of two replicates of independent experiments.

Figure 5. (a) MCF-7 3-D culture changes in growth and morphology induced by treatment with different combinations of **1**, CDDP and paclitaxel. Images have been acquired every other day, starting from day 0 on the Celigo imaging cytometer using Celigo software. Scale bar: 500 μm . (b) Changes in growth rate of MCF-7 spheroids treated with combination of CDDP and paclitaxel (open triangle), combination of **1** and paclitaxel (open circle), combination of **1** and CDDP (open square), combination of **1** with CDDP and paclitaxel (closed square), and non-treated control (full circle). Growth rate was determined by means of spheroid area established with Celigo software, and afterwards computed for days 4 and 8 by dividing the area on day-n with the area on day 0. Results are presented as the mean \pm SD of two replicates of independent experiments. (c) Type of interactions between drugs in combination treatments expressed by Combination index (CI), where $\text{CI} < 0.9$ indicates synergistic, $0.9 < \text{CI} < 1.1$ indicates additive, and $\text{CI} > 1.1$ indicates an antagonistic type of interaction. Results are presented as the mean \pm SD of two replicates of independent experiments.

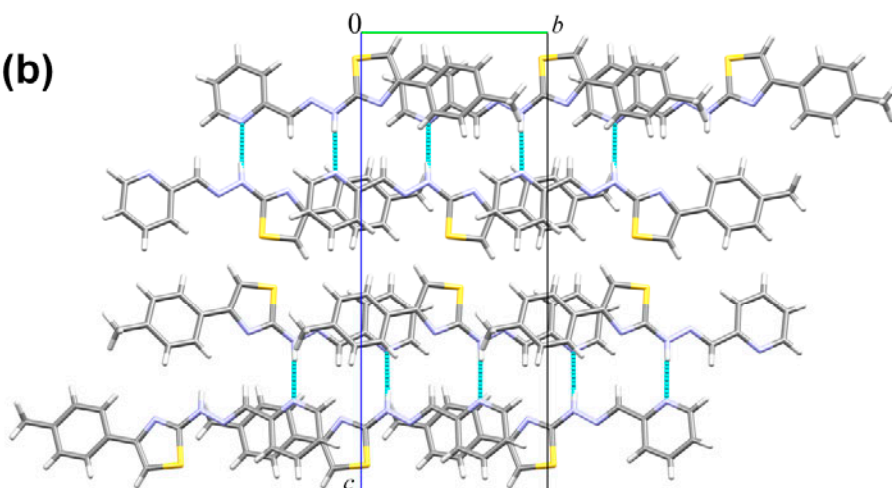


ACCEPTED MANUSCRIPT

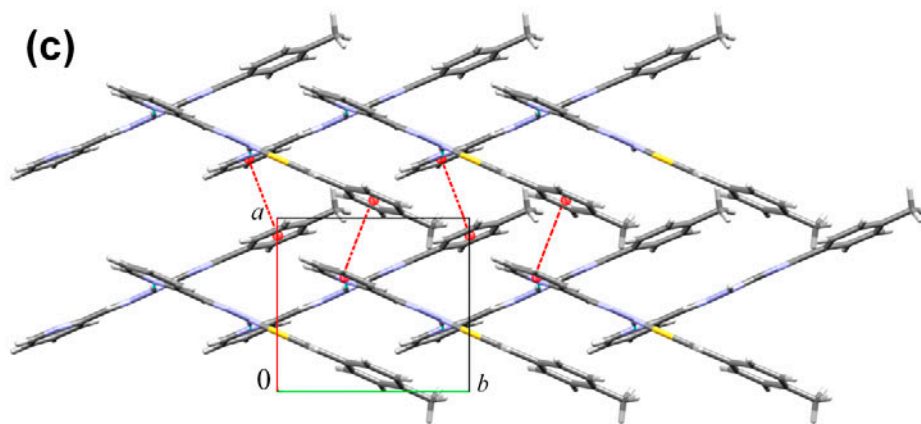
(a)



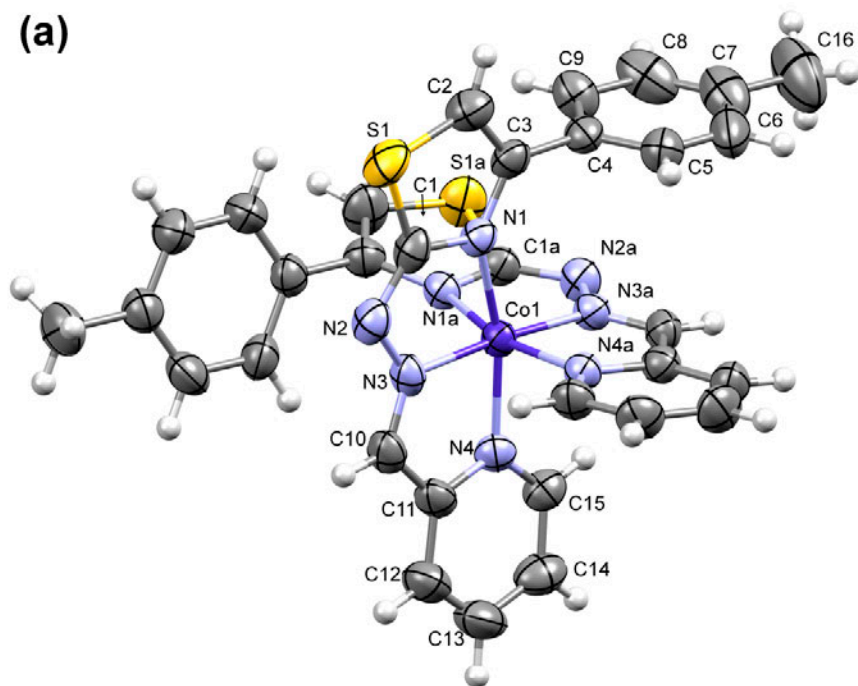
(b)



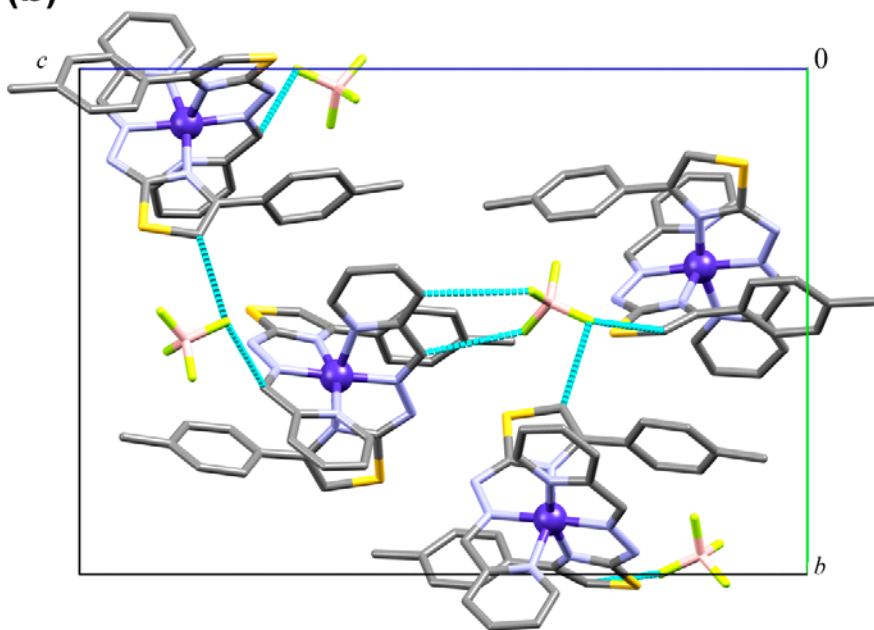
(c)

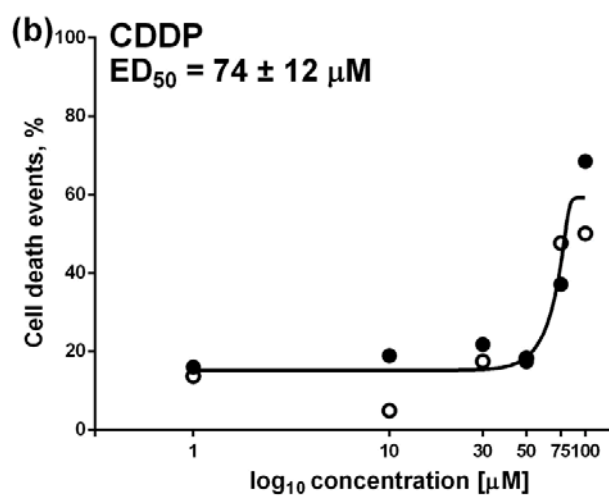
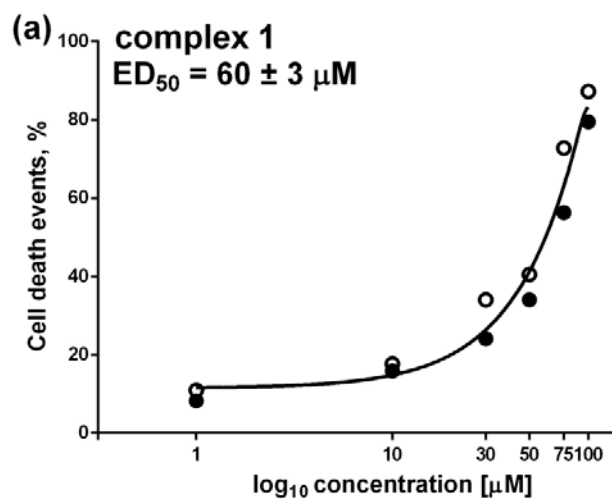


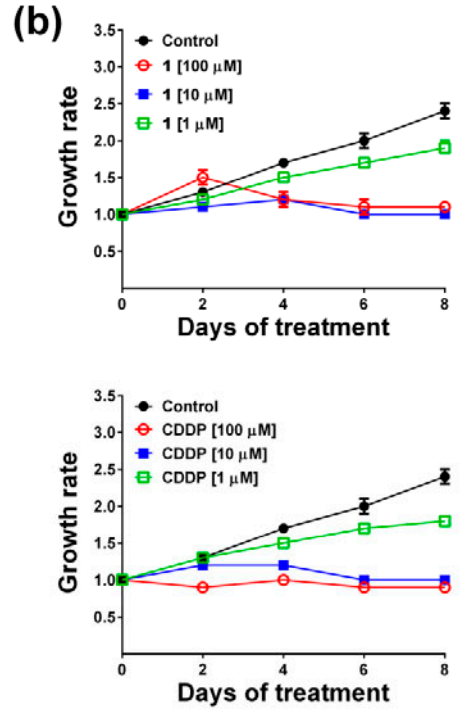
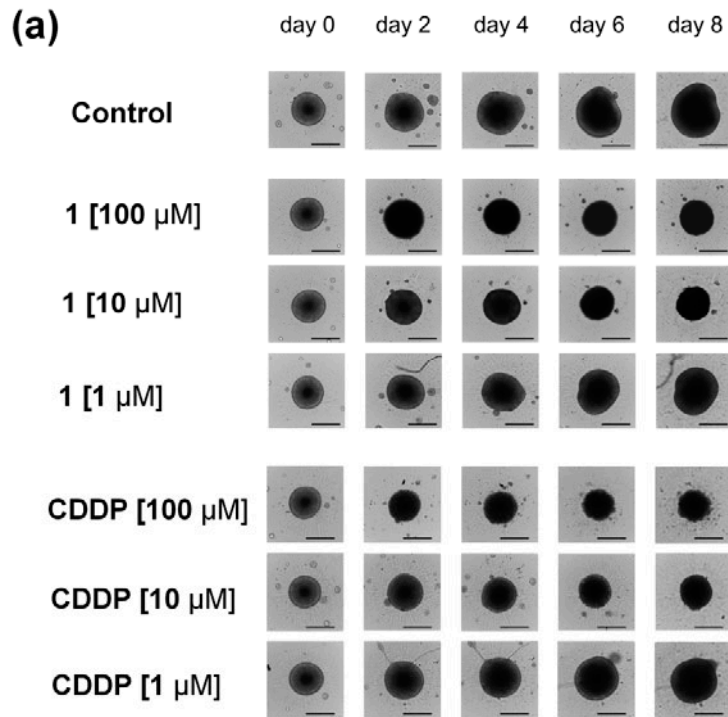
(a)



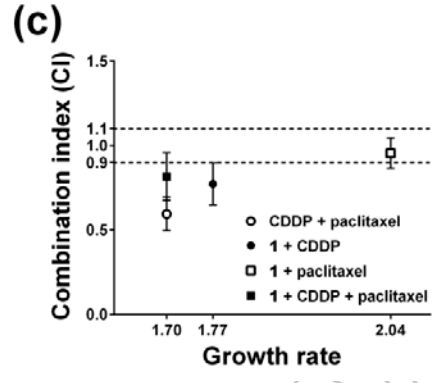
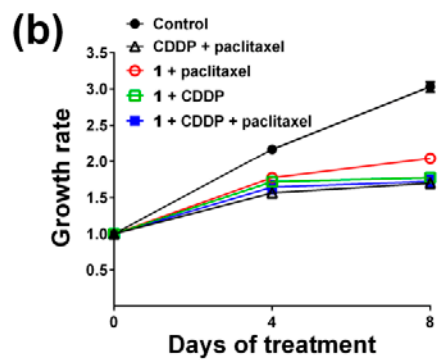
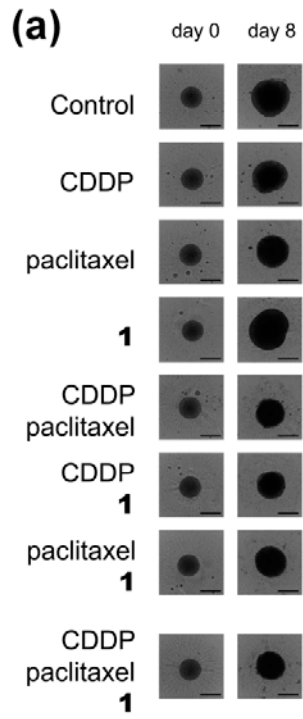
(b)



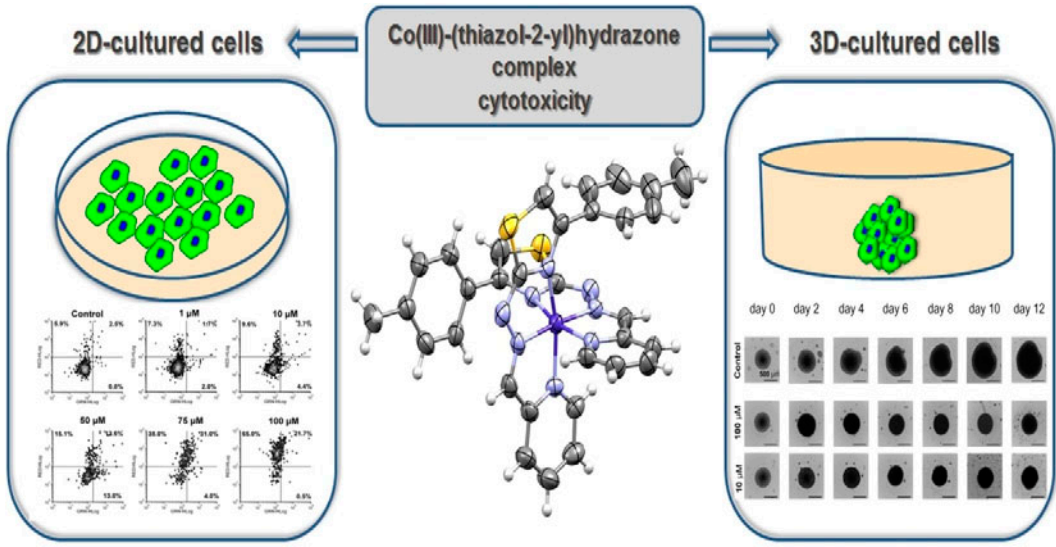




ACCEPTED MANUSCRIPT



ACCEPTED MANUSCRIPT



ACCEPTED MANUSCRIPT